

Particle Energies and Filling Fractions of Radio Bubbles in Cluster Cores

R.J.H. Dunn ^{*} and A.C. Fabian

Institute of Astronomy, Madingley Road, Cambridge CB3 0HA

23 October 2018

ABSTRACT

Using *Chandra* images of cluster cores with clear radio bubbles, we have determined k , which is the ratio of the total particle energy to that of the electrons radiating between 10 MHz and 10 GHz. Radiative and dynamical constraints on the bubbles indicate that the ratio of the energy factor, k , to the volume filling factor, f , lies within the range $1 \lesssim k/f \lesssim 1000$. Assuming pressure equilibrium between the radio-emitting plasma and the surrounding X-ray gas, none of the lobes have equipartition between relativistic particles and magnetic field. There is no evidence for any dependence of the upper limit of the k/f ratio on any physical parameter of the cluster or the radio source. The distribution of the upper limit on k/f appears to be bimodal, the value for some clusters being ~ 3 and for the others ~ 300 . We show that this is may due to the composition of the jet which forms the bubbles, the variation in the volume filling fraction or variation in the amount of re-acceleration occurring in the bubble.

Key words: galaxies: clusters – groups – X-rays: galaxies

1 INTRODUCTION

Radio lobes which emit synchrotron radiation contain relativistic electrons and magnetic fields. Disentangling the pressures of each component is difficult, and traditionally it has been assumed that there is equipartition between the particles and the field (Burbidge 1959), which corresponds closely to the minimum energy condition. Now, however, when the bubbles are embedded in an Intra Cluster Medium (ICM), this degeneracy can be removed by measuring the thermal pressure of the ICM and assuming pressure equilibrium between the bubbles and the surrounding X-ray gas as well as the lack of strong shocks. In particular, FR I sources in low redshift clusters imaged with *Chandra* often show holes in the X-ray emission coinciding with the radio lobes (e.g. Hydra A, (McNamara et al. 2000); Perseus, (Fabian et al. 2000); A2052, (Blanton et al. 2001); A2199, (Johnstone et al. 2002); Centaurus, (Sanders & Fabian 2002)), the first of which was discovered in the Perseus cluster with *ROSAT* (Böhringer et al. 1993). A recent compilation is given by Birzan et al. (2004).

Here we perform a detailed study of a sample of clusters which have clear radio bubbles. Following the approach first detailed in Fabian et al. (2002), we determine k/f , where k is the ratio of the total relativistic particle energy to that in electrons emitting synchrotron radiation between 10 MHz and 10 GHz, and f is the volume filling factor of the relativistic plasma in the bubble.

Fabian et al. (2002) calculated k/f for the northern radio bubble in the Perseus cluster and obtained a value of $180 < k/f < 500$. We find a value that is in broad agreement with theirs, and find

similar values for M84 and PKS 1404-267. However the remaining clusters in our sample, including A2052, A2199, A4059, Centaurus and Hydra A, appear to have much lower values. k/f appears to be either in the range $\sim 1 - 10$ or $\sim 100 - 1000$. We discuss the implications of this result on the evolution and formation of the bubbles. We use $H_0 = 70 \text{ km s}^{-1} \text{ Mpc}^{-1}$ throughout.

2 DATA ANALYSIS

We use standard synchrotron theory to quantify the properties of the particles present in the bubbles, following the analysis presented in Fabian et al. (2002). We give below some of the formulae required in order to define the variables. The total energy in relativistic electrons radiating between ν_1 to ν_2 , with a spectral index α ($S(\nu) \propto \nu^\alpha$), in a magnetic field B , producing a flux density S_ν at ν , is

$$E_e = 4\pi \times 10^{12} \left(\frac{cz}{H_0} \right)^2 \left(1 + \frac{z}{2} \right)^2 \frac{S_\nu \nu_2^{0.5+\alpha} - \nu_1^{0.5+\alpha}}{\nu^\alpha \alpha + 0.5} B^{-3/2} \\ \approx a B^{-3/2} \text{ erg}, \quad (1)$$

where $H_0 = 70 \text{ km s}^{-1} \text{ Mpc}^{-1}$. It has been assumed that the particle energy distribution extends from $\nu_1 = 10 \text{ MHz}$ to $\nu_2 = 10 \text{ GHz}$ as the radio images analysed were taken at frequencies between 1 and 8 GHz. Therefore the total energy in particles and magnetic field is

$$E_{\text{tot}} = kE_e + Vf \frac{B^2}{8\pi} = akB^{-3/2} + bfB^2 \text{ erg},$$

where V is the volume of the bubble, and f represents the volume filling factor of the relativistic plasma. k accounts for the additional

^{*} E-mail: rjhd2@ast.cam.ac.uk

energy from relativistic particles accompanying the electrons that radiate above 10 MHz and any non-relativistic component ($k = 1$ for an electron-positron plasma emitting only in the above waveband; a typical value used in the literature is $k = 100$). The bubbles are allowed to be aspherical, where r_l (“length”) is the radius along the jet direction and r_w (“width”) is the radius across the jet direction, where a symmetry axis has been assumed along the jet, hence the volume is $V = 4\pi r_l r_w^2 / 3$.

With the condition that there is simple equipartition between the energy present in particles and that present in the magnetic field, the magnetic field strength is

$$B_{\text{eq}} = \left(\frac{a}{b}\right)^{2/7} \left(\frac{k}{f}\right)^{2/7} \text{G}.$$

For the minimum energy magnetic field, replace $(a/b)^{2/7}$ with $(3a/4b)^{2/7}$ in the above equation.

If the relativistic gas is in equilibrium at equipartition with the thermal pressure from the gas in the rims surrounding the radio lobes (P_{th}), then the equipartition value, k/f_{eq} , can be obtained.

From now on we assume that the plasma is not in equipartition but still in pressure equilibrium, hence k/f can be found from

$$\frac{k}{f} = \left(P_{\text{th}} - \frac{B^2}{8\pi}\right) \frac{3V}{a} B^{3/2}. \quad (2)$$

To calculate k/f from Equation 2, estimates of the magnetic field strength in the bubbles are obtained from radiative and dynamical constraints.

A minimum value of $k/f = 1$ can be understood for an electron-positron plasma which fills all of the bubble. However, an extremal value can be determined by differentiating Equation 2, and finding the corresponding magnetic field gives a maximum value, k/f_{max} , which is 50% greater than the equipartition value. The absolute maximum value for the magnetic field is when $k/f = 1$ from when $(P_{\text{th}} - B^2/8\pi) \sim 0$, which is 1.53 times greater than the magnetic field at k/f_{max} , and 1.15 times the equipartition magnetic field. The field for k/f_{max} is the limit up to which the B^2 term can be ignored. Any further increase in B and this term becomes dominant and k/f decreases until it equals zero. After that the magnetic pressure is such that the bubble would be over pressured, even with $k = 1$, and for pressure equilibrium fewer particles than observed would be required.

A limit on the magnetic field present in the bubbles can be deduced from the fact that GHz radio emission is seen throughout the bubbles. Therefore the synchrotron cooling time of the relativistic electrons present is

$$t_{\text{sync}} = 2.7 \times 10^7 B_{-5}^{-3/2} \nu_9^{-1/2} \text{yr}, \quad (3)$$

where $B = 10^{-5} B_{-5} \text{G}$ and $\nu = 10^9 \nu_9 \text{Hz}$, has to be greater than the age of the bubble, assuming that there is no re-acceleration of the electrons in the bubble (for further discussion see Section 6.1). However Equation 3 is only valid for strong enough magnetic fields (for further discussion see Section 4.1).

The age of the bubble can be determined from the fact that the X-ray rims surrounding the radio bubbles appear not to be strongly shocked, hence they must be expanding at less than the sound speed of the gas in the rims, $c_s = \sqrt{\gamma kT/\mu m_{\text{H}}}$, where γ is the ratio of the heat capacities and $\mu = 0.62$. And therefore the age of the bubbles must be greater than $t_{\text{sound}} = 2r_l/c_s$ where r_l is the radius of the bubble. Twice the radius has been used as the bubble is blown from the radio source at the centre of the galaxy, which is at one edge of the bubble, rather than the centre, and so the “front edge”

travels twice the bubbles’ radius. This edge has travelled furthest during the lifetime of the bubble and so provides a limit on its age.

If the bubbles rise upwards at their buoyancy velocity, $v_b = \sqrt{2gV/SC_D}$, where S is the cross-sectional area of the bubble, V is the volume, $g = GM(< R_{\text{dist}})/R_{\text{dist}}^2$ for the bubble (centre) being at R_{dist} from the cluster core and $C_D = 0.75$ is the drag coefficient (Churazov et al. 2001), then the age of the bubble can be estimated as $t_{\text{buoy}} = R_{\text{dist}}/v_b$, the travel time to their current position. The enclosed mass was estimated from cluster mass profiles or using a linear interpolation from the Abell radius and mass as listed in Reiprich & Böhringer (2002). The latter is probably only correct to a factor of a few, though the uncertainty was taken into account in the calculation. The age of the bubble can also be estimated from the time required to refill the displaced volume as the bubble rises upward (McNamara et al. 2000), $t_{\text{refill}} = 2R_{\text{dist}} \sqrt{r/GM(< R_{\text{dist}})}$.

As the synchrotron lifetime of the GHz electrons must be greater than the age of the bubble, limits can be placed on the magnetic field, assuming that $\nu_9 = 1$.

The value obtained shows whether the equipartition solution is possible and allows k/f to be calculated from Equation 2. The limits obtained for k/f may be higher than the one predicted for equipartition. However, the equipartition condition is determined from the magnetic field strength, and Fig 7. of Fabian et al. (2002) shows that it is possible that limits on k/f are larger than the equipartition value even though the magnetic field is less than its equipartition value.

In the Perseus cluster there are weak shocks visible in the X-ray images (Fabian et al. 2000). Assuming that these have been created by the earlier supersonic expansion of the bubble, then a maximum age for the bubble can be estimated. Currently these shocks are travelling at the local sound speed, however, in the past the bubble that caused them was travelling supersonically, and so the average speed of the shocks over the bubble lifetime will be greater than the sound speed. Hence the age of the bubble must be less than $t_{\text{shock}} = R_{\text{shock}}/c_s$ where R_{shock} is the shock radius, centred on the central radio source.

Although this is an upper limit on the age of the bubble, there is no requirement that the synchrotron lifetime of the electrons is less than this value. However, in the assumption that it is, then this upper age limit, gives a lower limit on the magnetic field, and hence a lower limit on the value for k/f . In the Perseus cluster, which is the only cluster in the sample with a shock front visible, this limit together with the value obtained from the condition that there are no strong shocks at the rims gives the lowest range of k/f that can be understood from physical arguments.

Fabian et al. (2003b) showed that some of the H α filaments seen in the Perseus cluster could be interpreted as streamlines behind the western “ghost” bubble. This indicated that the flow is laminar, and implies a Reynolds number of less than 1000. Using this, a value of $4 \times 10^{27} \text{cm}^2 \text{s}^{-1}$ was obtained for the kinematic viscosity. The Reynolds number, Re , was calculated for each bubble analysed, assuming the viscosity was the above value, and also a lower bound on the viscosity was calculated from the limit on the Reynolds number of 1000 assuming that the flow is laminar in each cluster.

2.1 Non-uniform Magnetic Fields

It is unlikely that the magnetic fields present in the bubbles are completely uniform over the entire bubble. The effect of non-uniform magnetic fields was investigated very simply, using a centrally

Table 1. : EFFECT OF NON-UNIFORM MAGNETIC FIELD ON k/f

Cluster Lobe	Timescale	Uniform Field	Non-uniform Field
Perseus North	Sound	573	1083
	Shock	390	735
Perseus South	Sound	1025	1937
	Shock	762	1436

NOTES:

 The limits on k/f for the sound speed and shock calculations from the Perseus Cluster with a uniform and non-uniform magnetic field.

peaked linear distribution ($B \propto -|r|$). This gave limits on k/f that were a factor of two greater than if a uniform magnetic field was used, for the case of Perseus (Table 1). It was checked that the calculation used for the non-uniform field produced the same limits on k/f for the a uniform field as were produced from the other calculations.

2.2 Energetics

The energies and powers were also calculated, using $E = PV$ for the energy, and $\mathcal{P} = E/t$ for the powers using all of the timescales calculated above. However, if the energy required to expand the bubble as well as the energy in the bubble is accounted for, then, for slow expansion rates:

$$E = \frac{1}{\gamma - 1}PV + PdV \approx \frac{\gamma}{\gamma - 1}PV,$$

where V is the volume of the bubble and γ is the mean adiabatic index of the fluid in the bubble (5/3 for non-relativistic gas or 4/3 for relativistic gas). For the relativistic case (assumed as there is synchrotron emission in the cavity) this increases the energy by a factor of 4 (5/2 for non-relativistic), and hence also the power. Therefore the values for the energy in Table 3 should be multiplied by the appropriate $\gamma/(\gamma - 1)$.

3 DYNAMICAL CONSTRAINTS

PdV work is done by the bubble on its surroundings during its expansion, equating to a power $\mathcal{P} \approx P_{th}fV/t$. The jet must be powerful enough to inflate the holes, and an estimation of this power can be obtained by considering the evolution of the expanding bubble in a medium of constant pressure (Churazov et al. 2001, 2000). We modify their expressions for the expansion of the bubble to include the effect of gas clumping through the volume filling factor. From the internal energy of the hole and the compression of the surrounding gas during subsonic expansion

$$\frac{\mathcal{P}t}{P_{th}f} = V \frac{\gamma}{\gamma - 1} = F, \quad (4)$$

where γ for the radio-emitting plasma is assumed to be 4/3. Secondly, from the condition that there are no strong shocks at the bubble rims, the expansion rate must be subsonic, and so

$$\frac{\mathcal{P}}{P_{th}ft^2} < 36\pi c_s^3 \frac{\gamma}{\gamma - 1} = G. \quad (5)$$

Finally, assuming that the bubble has not detached from the source, which seems to be the case for the majority of the clusters, then its

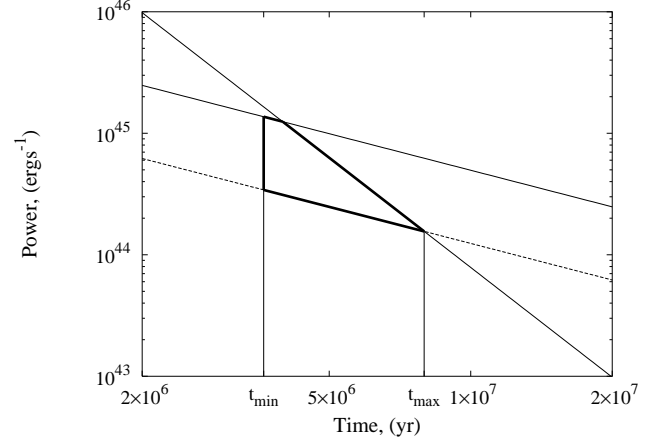


Figure 1. The dynamical constraints given in Section 3 shown for the northern Perseus bubble. The vertical lines show the minimum t_{min} , obtained from the combination of the energy and sound speed equations (4) and (5), and maximum t_{max} ages of the bubble, obtained from the combination of the energy and buoyancy equations (4) and (6). The inclined lines show the limits on the power of the source, the upper shallow line is from Equation 4 and the steep line is from Equation 7. The dotted shallow line represents the minimum power required to move the gas to make the hole ($P_{th}V/t$). In all the equations, f has been taken as 1, and P_{th} is the value obtained from the temperature and density of the bubbles.

velocity is less than the buoyancy velocity, giving

$$\begin{aligned} \mathcal{P} &= \frac{36\pi\gamma}{\gamma - 1} \left(\frac{8}{3C_D} \right)^{3/2} \left(\frac{r}{R} \right)^{3/2} \left(\frac{GM(<R)}{R} \right)^{3/2} P_{th}t^2 f^{5/2} \\ &= HP_{th}t^2 f^{5/2}. \end{aligned} \quad (6)$$

Combining these expressions produces other limits on the ages of the radio bubbles — (4) and (5) produce a minimum age for the hole, $t_{min} = (F/G)^{1/3}$; and (4) and (6) lead to a relation

$$\mathcal{P} < H^{-2/3} F^{5/3} P_{th}t^{-3}. \quad (7)$$

There is also a minimum power for the source, from $P_{th}V/t$ for $f = 1$. The intersection of this with (7) gives the maximum age of the hole as

$$t_{max} = \sqrt{\frac{F^{5/3} H^{-2/3}}{V}}.$$

These relations are only valid for subsonic expansion. For Perseus at least, there exists a weak shock indicating that there has been supersonic expansion in the past (Fabian et al. 2003a). Therefore the agreement between the timescales given by these relations, with the ones drawn from the other physical arguments may give a crude indication of what proportion of its lifetime the bubble has spent in subsonic expansion. The allowed region for the bubble from these constraints in the Power–Age plot in Fig. 1 is the highlighted polygon defined by the minimum and maximum ages, the power limits from Equations 4 and 7 and the minimum power for the source.

4 RESULTS

The individual source properties are listed in Table 2. In A2199, the inner jet-like feature visible on the radio overlays in Johnstone et al. (1998) has small X-ray depressions associated with the knots at the ends of the jet (Inner East (I-E) and Inner West (I-W)), and these were analysed separately from the extended primary emission. If

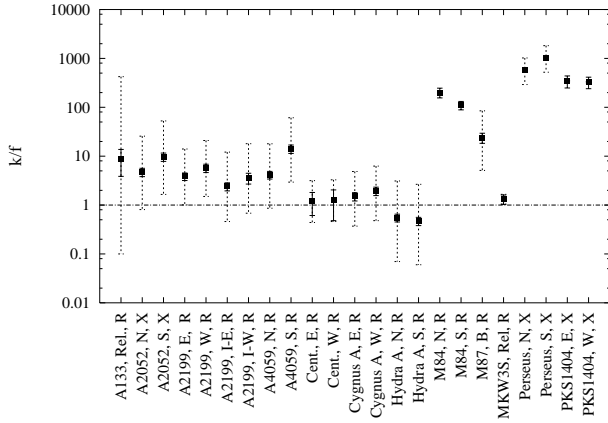


Figure 2. The value of k/f calculated from the sound speed limit for each cluster analysed, along with the uncertainties arising from the uncertainties in α (the dotted bars) and from the uncertainties in the other physical parameters of the source (the solid bars). The dotted line shows the minimum value of k/f possible from the assumptions used in the calculations.

the source has prominent X-ray rims around the radio bubbles, e.g. Perseus, then these have been used to define the size of the bubbles. Otherwise the spatial extent of the radio emission has been used to define the size of the radio bubble. In some cases the GHz radio emission does not entirely fill the X-ray defined holes - e.g. A2052. In Cygnus A, the fluxes used in the calculation do not include the hotspots at the end of the jet, to reduce the effect of re-acceleration of electrons (for further discussion see Section 6.1).

The limits on k/f calculated from the different timescales are tabulated in Table 3. Ignoring the uncertainties in the limits on k/f , Perseus has the smallest range in k/f as the two constraints come from the weak shock (k/f_{shock}) and the lack of strong shocks in the rims (k/f_{sound}). However the ranges in k/f for the Northern ($390 < k/f < 570$) and Southern ($760 < k/f < 1025$) bubbles do not overlap, which is surprising. However, if the uncertainties in the individual limits are also included, then the ranges are much larger, and do overlap ($200 < k/f < 1020$ and $390 < k/f < 1830$). The values obtained are in agreement with the range of $180 < k/f < 500$ obtained by Fabian et al. (2002) for the northern bubble. This is assuming that the synchrotron lifetime is less than the maximum age of the bubble, but there is no physical requirement that this is the case. All other clusters have an upper limit on k/f arising from the sound speed limit and two other limits from physical arguments (buoyancy and refilling timescales).

The maximum and minimum values in the table above come from the uncertainties in the values of the spectral index, α , over the radio lobe. The resultant uncertainty in k/f from the uncertainty in α can be greater than an order of magnitude as the spectral index appears as an exponent in Equation 1. There are uncertainties in k/f which come from the uncertainties in the other observed values, however for most of the clusters these are much smaller than the uncertainties from the those in α . The limits on k/f calculated from the lack of strong shocks in the rims (sound speed limit) is plotted in Fig. 2 with the uncertainties in the limits on k/f arising from the ranges in α and those from other uncertainties plotted separately. The dotted line demarcates the minimum value possible for the assumptions used in the calculations. Each lobe is plotted separately, identified by the same label as in Tables 2 and 3.

The uncertainties in the spectral index are generous — α

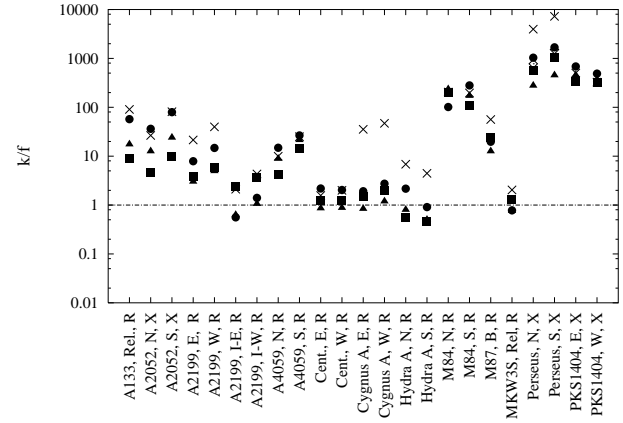


Figure 3. The value of k/f for each cluster analysed. The \blacksquare , \blacktriangle , \bullet and \diamond symbols denote the k/f values from the sound speed, shock, buoyancy and refilling timescales respectively. The \times symbol denotes the equipartition values

varies across the radio lobes, and so an average value has been taken, with an uncertainty to cover the range. In some cases the values stated by different authors do not match, and again an average has been taken, with the range encompassing the values.

The variation in the limits on k/f obtained from the different timescales is shown in Fig. 3. On the whole, the k/f limiting values from different timescales fall within the range of k/f_{sound} given by the uncertainties in α . It was not expected that the values would be exactly the same, but for about half of the clusters the differences are less than $\sim \times 2.0$. The remainders' are less than $\sim \times 8$ and these disagreements arise primarily from differences in the timescales calculated (for further discussion see Section 4.1). As the values obtained for the limits on k/f from these different arguments are on the whole similar, it implies that the actual limits on k/f are around those values. However all the values have uncertainties of the same size as for the sound speed (they have not been plotted for clarity), which reduces the reliability of this conclusion.

For most of the bubbles, radio images at different frequencies were obtained, and a separate limit on k/f was calculated for each. The resultant values usually were all but identical, and certainly agreed to within the uncertainties arising from all values apart from the spectral index, however they have not been tabulated in this work for brevity and clarity. It was checked to see if the frequency at which the flux was measured had some effect on the limit on k/f , but none was found. In the clusters where two bubbles are visible, their k/f limits broadly agree to within the uncertainties

4.1 Timescales

The timescales (ages) for each lobe were calculated during the course of this work. The differences between our values and those presented in the literature come mainly from the different sizes of the bubbles used, and different cosmologies. They have been tabulated in the Appendix along with the powers of the sources which have been calculated from these timescales.

For some of the bubbles the timescales obtained by the different estimates differ by up to a factor of 10. These discrepancies are probably due to the assumptions used in the calculation of the timescales.

The sound speed timescale relies on the fact that the bubble is

Table 2. : SOURCE PROPERTIES

Cluster	Lobe ⁽¹⁾	Redshift	α	$\log(P_5 \text{ GHz})$ (W/Hz)	$R_{\text{dist}}^{(2)}$ (kpc)	r_1 (kpc)	r_w (kpc)	R_{shock} (kpc)	M_{encl} ($10^{12} M_{\odot}$)	kT (eV)	n_e (cm^{-3})	References
A133	Rel, R	0.054	-2.0 ± 1.0	23.0	40.0	50.0	20.0	-	8.0	2400	0.01	1,2,3,4,5,6,7
A2052	N, X S, X	0.035	-1.6 ± 0.3	24.7	10.0 15.0	10.0 15.0	10.0 15.0	- -	4.0 5.0	1100 1100	0.049 0.049	7,8,9,10,11,12,13,14
A2199	E, R W, R I-E, R I-W, R	0.031	-1.9 ± 0.3	24.3	20.2 21.5 4.23 4.23	16.9 20.9 1.0 1.5	12.2 14.4 1.0 1.5	- - - -	1.6 1.7 0.08 0.08	3100 3200 2050 2050	0.017 0.017 0.056 0.056	13,15,16,17
A4059	N, R S, R	0.050	-1.4 ± 0.3	24.0	5.44 3.92	5.44 3.92	2.98 4.48	- -	1.5 1.1	2000 2000	0.028 0.028	7,13,14,18,19
Centaurus	E, R E, R	0.010	-1.3 ± 0.2	25.8	1.45 2.00	1.45 1.88	1.13 1.02	- -	0.020 0.025	800 1000	0.09 0.08	13,20
Cygnus A	E, R W, R	0.056	-1.0 ± 0.3	27.7	44.1 48.0	30.3 33.9	23.7 25.2	- -	3.0 5.0	4000 5500	0.05 0.04	13,21,22,23,24
Hydra A	N, R S, R	0.052	-1.2 ± 0.4	26.3	17.8 22.2	20.0 16.7	8.5 6.9	- -	2.0 2.0	2900 3000	0.041 0.036	13,25,26,27
M84	N, R S, R	0.0035	-0.51 ± 0.02	22.0	2.7 3.8	2.1 4.0	2.5 2.6	- -	0.2 0.2	650 650	0.04 0.04	28,29,30
M87	Bud, R	0.0044	-1.2 ± 0.4	24.4	3.11	1.31	1.31	-	0.14	1500	0.20	13,31
MKW3s	Rel, R	0.045	-2.7 ± 0.05	23.8	56.4	12.9	17.9	-	16.0	3200	0.004	7,32,33
Perseus	N, X S, X	0.018	-1.0 ± 0.2	25.9	8.15 8.89	8.15 8.89	8.15 8.89	24.0 24.0	0.24 0.26	2604 3175	0.064 0.055	13,34,35,36,37,38
PKS 1404	E, X W, X	0.022	-0.39 ± 0.03	23.8	3.94 2.75	2.29 1.33	1.58 1.7	- -	0.40 0.40	930 820	0.056 0.066	39,40,41,42

REFERENCES:

(1) Fujita et al. (2002); (2) Slee et al. (2001); (3) Owen & Ledlow (1997); (4) Rizza et al. (2000); (5) Slee & Reynolds (1984); (6) Komissarov & Gubanov (1994); (7) Reiprich & Böhringer (2002); (8) Blanton et al. (2001); (9) Blanton et al. (2003); (10) Burns (1990); (11) Stefanachi et al. (2002); (12) Zhao et al. (1993); (13) Taylor et al. (2002); (14) G. Taylor, private comm. (2004); (15) Johnstone et al. (2002); (16) Andernach et al. (1988); (17) Burns et al. (1983); (18) Choi et al. (2004); (19) Taylor et al. (1994); (20) Sanders & Fabian (2002); (21) Perley et al. (1984); (22) Carilli et al. (1991); (23) Smith et al. (2002); (24) Alexander et al. (1984); (25) McNamara et al. (2000); (26) Taylor et al. (1990); (27) Voigt & Fabian (2004); (28) Finoguenov & Jones (2002); (29) Teräsrananta et al. (2001); (30) Cao & Rawlings (2004); (31) Forman et al. (2003); (32) Mazzotta et al. (2002); (33) McNamara et al. (1990); (34) Fabian et al. (2002); (35) Fabian et al. (2000); (36) Fabian et al. (2003b); (37) Voigt & Fabian (2004); (38) Pedlar et al. (1990); (39) Drinkwater et al. (1997); (40) Johnstone et al. (1998); (41) Brown & Burns (1991); (42) Bettoni et al. (2003)

NOTES:

(1) The codes for the Lobes are N—Northern, S—Southern, E—Eastern, W—Western, X—sizes from X-ray image, R—sizes from Radio image, I-E/W—Inner lobes in A2199, Bud—as described in Forman et al. (2003), Rel—Relic source (for A133 as described in Fujita et al. (2002)).

(2) All the values given in the above table except the radio power have an uncertainty associated with them. Except for the spectral index, they are not quoted as they have limited effect on the calculated values. The effect of the uncertainties in α on the resultant uncertainties in k/f is large and so are stated here. For further discussion see text.

not currently expanding supersonically and gives the time for the expansion of the bubble. From the observation that there are no strong shocks at the rims we have assumed that the average expansion speed was less than the current sound speed over the lifetime of the bubble. However, as we assume that the bubble is produced by a relativistic jet and the presence of the shock in the X-ray images of the Perseus cluster, the earlier expansion of the bubble must have been supersonic, and so this lower limit on the timescale may be an overestimate. The lack of strong shocks in the rims still allows some supersonic motion, Blanton et al. (2001) state that $\mathcal{M}a < 1.2$

for A2052, so the sound speed may be an underestimate of the expansion speed.

The buoyancy timescale used is the time taken for a bubble of the size observed to rise at its buoyancy velocity from the centre of the gravitational potential to its current position, i.e. by its own radius. This is calculated assuming that the surrounding ICM is at a constant pressure and density. However as the bubble is expanding as it ages, the initial stages are probably supersonic, the medium through which it rises is likely to be non-uniform and in some cases the masses used in the calculation are estimates; the

Table 3. PHYSICAL k/f VALUES

Cluster	Lobe ⁽¹⁾	Pressure (eV/cm ³)	Re	Viscosity ⁽²⁾ (10 ²⁷ cm ² s ⁻¹)	Energy ⁽³⁾ (10 ⁵⁸ erg)	k/f_{eq}	$k/f_{sound}^{(4)}$	k/f_{shock}	$k/f_{buoyancy}$	k/f_{refill}
A133	Rel, R	52.8	4106	16.4	20.8	90.6	8.79 ⁴²⁴ _{0.10}	—	57.3 ²⁷⁶⁰ _{0.68}	17.5 ⁸⁴³ _{0.21}
A2052	N, X	119	367	3.83	2.3	26.6	4.73 ^{25.7} _{0.81}	—	36.3 ¹⁹⁷ _{6.19}	12.6 ^{68.6} _{2.15}
	S, X	119	551	4.69	7.9	81.3	9.68 ^{52.6} _{1.65}	—	79.7 ⁴³³ _{13.6}	24.0 ¹³¹ _{4.10}
A2199	E, R	116	754	3.77	4.2	21.5	3.85 ^{14.0} _{1.01}	—	7.90 ^{28.8} _{2.07}	3.02 ^{11.0} _{0.79}
	W, R	120	904	4.90	7.1	39.8	5.74 ^{21.0} _{1.50}	—	14.8 ^{53.9} _{3.87}	4.97 ^{18.1} _{1.30}
	I-E, R	253	50.1	0.08	0.005	2.11	2.40 ^{12.1} _{0.46}	—	0.56 ^{2.84} _{0.11}	0.63 ^{3.17} _{0.12}
	I-W, R	253	75.2	0.15	0.017	4.32	3.58 ^{18.0} _{0.68}	—	1.40 ^{7.06} _{0.274}	1.06 ^{5.32} _{0.20}
A4059	N, R	123	148	0.69	0.065	9.97	4.15 ^{18.0} _{0.86}	—	14.9 ^{64.4} _{3.10}	8.85 ^{38.3} _{1.84}
	S, R	123	222	1.22	0.22	25.0	14.1 ^{61.1} _{2.94}	—	26.6 ¹¹⁵ _{5.53}	21.5 ^{93.0} _{4.47}
Centaurus	E, R	158	35.3	0.16	0.0045	1.57	1.21 ^{3.16} _{0.44}	—	2.18 ^{5.67} _{0.79}	0.86 ^{2.25} _{0.31}
	E, R	176	35.7	0.13	0.0037	2.00	1.26 ^{3.28} _{0.46}	—	2.03 ^{5.29} _{0.74}	0.88 ^{2.28} _{0.32}
Cygnus A	E, R	440	1552	6.21	116.0	35.5	1.50 ⁴⁸⁶ _{0.37}	—	1.92 ^{6.23} _{0.48}	0.84 ^{2.72} _{0.21}
	W, R	484	2066	8.26	152.0	46.9	1.94 ^{6.27} _{0.48}	—	2.73 ^{8.84} _{0.68}	1.19 ^{3.86} _{0.30}
Hydra A	N, R	264	507	3.64	3.2	6.84	0.55 ^{3.11} _{0.07}	—	2.16 ^{12.2} _{0.29}	0.80 ^{4.53} _{0.11}
	S, R	238	416	2.16	1.5	4.45	0.47 ^{2.65} _{0.06}	—	0.91 ^{5.13} _{0.12}	0.50 ^{0.84} _{0.07}
M84	N, R	57.2	71.8	0.52	0.019	205	201 ²⁰⁷ ₁₉₄	—	101 ¹⁰⁴ _{98.1}	268 ²⁷⁶ ₂₅₉
	S, R	57.2	73.5	0.52	0.020	196	110 ¹¹⁴ ₁₀₇	—	298 ²⁹⁶ ₂₇₉	202 ²⁰⁸ ₁₉₅
M87	Bud, R	660	56.2	0.22	0.029	56.2	23.9 ^{84.7} _{5.11}	—	19.7 ^{70.0} _{4.22}	12.6 ^{44.7} _{2.70}
MKW3s	S, R	28.2	1118	5.50	3.2	2.04	1.32 ^{1.66} _{1.05}	—	0.78 ^{0.97} _{0.62}	0.76 ^{0.96} _{0.61}
Perseus	N, X	367	460	1.68	3.9	3966	573 ¹⁰²⁰ ₂₉₂	390 ⁶⁹⁶ ₁₉₉	1031 ¹⁸³⁹ ₅₂₆	278 ⁴⁹⁶ ₁₄₂
	S, X	384	555	1.84	5.3	7262	1025 ¹⁸²⁷ ₅₂₂	762 ¹³⁵⁷ ₃₈₈	1682 ²⁹⁹⁹ ₈₅₇	453 ⁸⁰⁷ ₂₃₁
PKS1404	E, X	115	53.5	0.47	0.009	503	343 ³⁵⁴ ₃₃₂	—	685 ⁷⁰⁷ ₆₆₂	454 ⁴⁶⁸ ₃₈₄
	W, X	118	53.7	0.55	0.011	327	327 ³³⁷ ₃₁₆	—	487 ⁵⁰² ₄₇₀	372 ³⁸⁴ ₃₅₉

NOTES:

(1) The codes for the Lobes are N—Northern, S—Southern, E—Eastern, W—Western, X—sizes from X-ray image, R—sizes from Radio image, I-E/W—Inner lobes in A2199, Bud—as described in Forman et al. (2003), Rel—Relic source (for A133 as described in Fujita et al. (2002)).

(2) The viscosity is estimated assuming that the flow is laminar and a Reynolds number of 1000

(3) The energy quoted here is $E = PV$, so the values have to be multiplied by the appropriate $\gamma/(\gamma - 1)$.

(4) The range on the limits on k/f from the uncertainty in the spectral index are given by the maximum values (superscript) and minimum values (subscript). The uncertainties from other parameters are shown in Fig. 2.

buoyancy velocity will change with the evolution of the bubble, and so the timescale has uncertainties associated with it.

These two timescales are measuring the age of the bubbles in two different ways, one the time for expansion to the current size at the sound speed of the ICM at the edge of the bubble; the other the time to travel to the current position at the buoyancy velocity. This, along with the fact that calculation for the expansion (sound speed) timescale uses twice the radius (see Section 2) is the most likely cause of the discrepancies between the timescales. From the geometry of the bubbles, we have assumed that the engine creating the bubble is not in the centre, but at one side. Therefore the part of the bubble which is furthest from the source, the bubbles' diameter away, is the part whose speed must have been less than the sound speed.

In very young bubbles are the sound speed timescales less than the buoyancy timescales e.g. M87 and A2199 (though these seem to be expanding at a large distance from the central engine, and

hence the comparatively large buoyancy timescale). The older, and usually larger, bubbles have buoyancy timescales which vary from about equal (Cygnus A) to ten times smaller than the sound speed timescale (A133).

Both the buoyancy and refilling timescales depend upon the cluster mass within the radius the bubbles are from the centre. In the cases of A133 and A4059, the masses have been estimated from a linear interpolation of the Abell radius as given in Reiprich & Böhringer (2002) and so the value obtained is likely to be accurate only to factors of two to three. In addition, Slee et al. (2001) also find that the travel time of the relic in A133 is longer than its age, a discrepancy which they propose can be resolved by identifying the relic not with the cD galaxy, but the one labelled as G in their Figure 6, which gives a travel time of around the age of the relic. The relic does seem to be much larger than others given its distance from the centre of the cluster, and so projection effects may also play a part. The timescales for A4059 also dif-

fer by factors of up to three, and if the mass estimate is reduced from $1.5/1.1 \times 10^{14} M_{\odot}$ for the Northern and Southern bubbles respectively to $\sim 0.20 \times 10^{14} M_{\odot}$, then the timescales become more comparable ($\times 3$ compared to $\times 6$ different). This is a reduction of $\sim 90\%$, however a linear interpolation of the mass from the Abell radius overestimates the masses of Perseus and A2199 (inner bubbles) by more than a factor of ten. These new masses for A4059 give $t_{\text{buoy}} = 0.71 \times 10^7$ yr, $t_{\text{ref}} = 2.0 \times 10^7$ yr, $k/f_{\text{buoy}} = 8.9$ and $k/f_{\text{ref}} = 3.51$ for the Northern bubble and $t_{\text{buoy}} = 0.43 \times 10^7$ yr, $t_{\text{ref}} = 1.7 \times 10^7$ yr, $k/f_{\text{buoy}} = 31.9$ and $k/f_{\text{ref}} = 9.92$ for Southern bubble. The k/f values do not change radically ($\sim 50\%$ drop) as a result of this.

The form for the synchrotron lifetime (Equation 3) is only valid for sufficiently large magnetic fields. Inverse Compton (IC) losses dominate when the energy density of the Cosmic Microwave Background is equal to that of the magnetic field, $U_B = B^2/8\pi$, which corresponds to $B = B_{\text{CMB}}$. Although all the clusters analysed are in the local Universe, it was checked whether the inferred magnetic field was larger than B_{CMB} . The lifetime determined from this limiting magnetic field for 1 GHz electrons (t_{CMB}) was also calculated and is tabulated in the Appendix. Only A133 has a timescale, inferred from the sound speed, that is larger than t_{CMB} . The magnetic field is also smaller than B_{CMB} , and so IC losses are important in this cluster. The Eastern lobe of Cygnus A has a magnetic field from the refilling timescales that is less than 10% larger, and so IC losses may be important in this cluster as well.

The sound speed timescale gives a lower limit on the age, and hence an upper limit on the magnetic field, and so the IC effects are likely to be important for more clusters than just the two mentioned above, as the actual age of the bubble is probably larger, and so the magnetic field smaller.

5 DISCUSSION

Initially it had been hoped that limits on k/f for the clusters were all of the same order of magnitude, however, from Fig. 2 it is apparent that they are not. The minimum possible value for $k/f = 1$ is shown by the dotted line. Hydra A is the only source whose k/f value falls below this line, though the uncertainties are such that it could have a value greater than one. A possible reason for this source having such a low k/f value is that the bubbles may have punched their way through the ICM. Therefore the bubbles are no longer being contained and so are no longer in the type of equilibrium that has been assumed in the calculations.

The calculations have shown that all the lobes cannot be in equipartition. Although some of the limits on k/f are larger than the equipartition k/f values, this is due to the form of the dependence of k/f on the magnetic field (see Fig. 7 of Fabian et al. (2002)). All the timescales derived from observational data indicate that the bubbles cannot be in equipartition. The only timescales that allow equipartition are the minimum and maximum from the dynamical constraints (Section 3), and only for some clusters.

The limits on k/f from the maximum and minimum ages of the hole as calculated from the dynamical constraints arguments in Section 2 are shown in Fig. 4, along with the equipartition values and the sound speed limits for comparison. These limits are higher than the ones obtained from the sound speed for many clusters. This implies that the assumptions used in the calculation of these limits on k/f may not be valid. Another indication that this may be so is the fact that the timescales are inconsistent with each other — the maximum age of the hole is frequently less than the minimum age

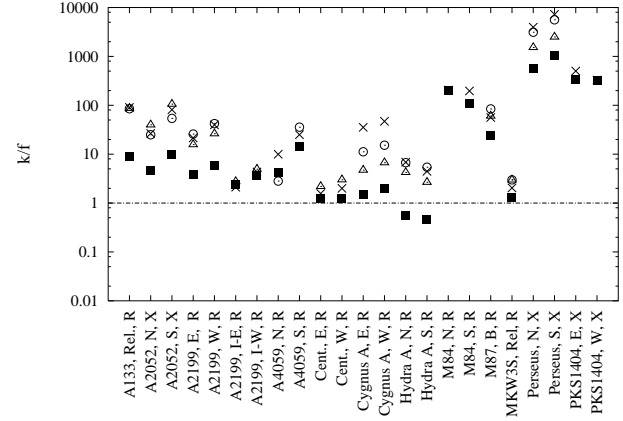


Figure 4. The value of k/f for each cluster analysed. The ■, ○ and △ symbols denote the k/f values from the sound speed, minimum and maximum timescales respectively (Section 1). The × symbol denotes the equipartition values.

of the hole (see the Appendix for the values), and, on the whole, both are less than the sound speed values. This can be seen in Fig. 1 where the maximum allowed age for the northern bubble in the Perseus cluster is less than 10^7 years, whereas the values calculated from the sound speed and shock front arguments give 2.2×10^7 and 3.2×10^7 years respectively. We therefore believe that the assumptions made in the derivation and calculation of these values are not valid for these bubbles. The largest assumption are that the bubbles have been expanding sub-sonically and in a medium of constant pressure, which is unlikely, as there is a shock front visible in the Perseus X-ray images and the temperature and density of the ICM varies with distance from the centre of the cluster. Another assumption used is that they have not buoyantly detached from the source, which in some cases must have occurred (e.g. A133 and MKW3s).

Although the k/f values calculated are upper limits, treating them as absolute values, it was investigated if there was any distribution of k/f with the physical parameters of the sources. The only parameters which came up with possible trends were the electron density, the 5 GHz radio power of the source and the spectral index of the lobes (Figs. 5, 6 and 7). In the plot of k/f against electron density there seems to be a cut-off line from the lower left to the upper right-hand side of the scatter plot, with all the clusters falling to the right of this line. There seems to be a trend with 5 GHz radio power, with low power sources having a high k/f , and high power sources having a low k/f . However the Perseus cluster is an exception to this last trend (the points with a $k/f \sim 500$ at a radio power of $\sim 3 \times 10^{25} \text{ W Hz}^{-1}$). Any effect from beaming has not been taken into account, but as the bubbles seem to be moving across the line of sight, it is unlikely that there are large beaming effects. A similar trend may be present in the plot of k/f versus α . It is also obvious in this plot of the large effect an uncertainty in the spectral index has on the uncertainty in k/f . In the above discussion the uncertainties on k/f values have not been taken into account, however due to the size of the uncertainties any firm conclusions being drawn from the plots. We believe that there is no clear correlation of k/f with any physical parameter of the bubble.

As there was no firm trend of k/f with any of the physical parameters of the lobes or the source, other possible distributions were looked for, and it was noticed that the k/f_{sound} values were clustered - the value for some clusters occurred around 3 and others occurred around 300. The number of bubbles with

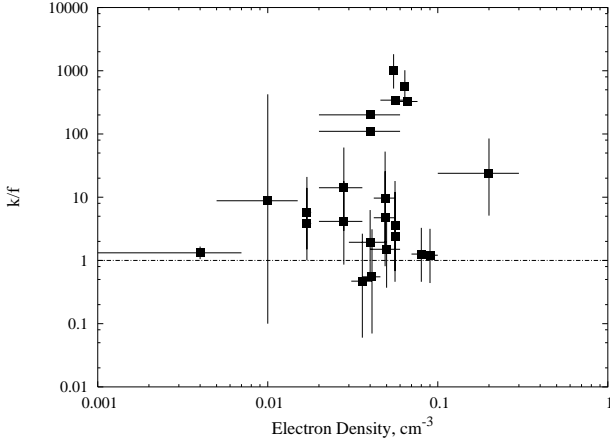


Figure 5. The distribution of k/f versus electron density. The errors in k/f come from the uncertainty in α .

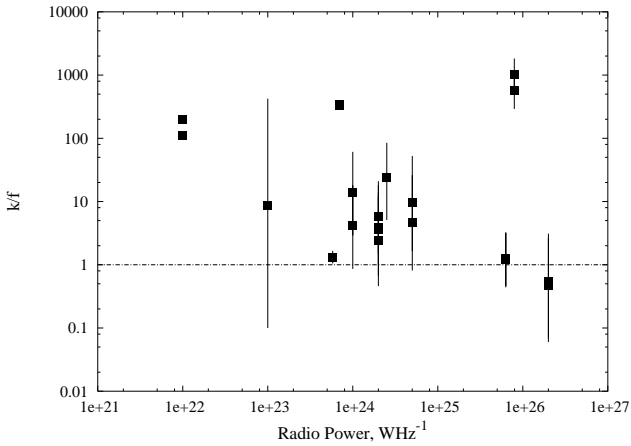


Figure 6. The distribution of k/f versus the radio power of the source at 5 GHz. The errors in k/f come from the uncertainty in α .

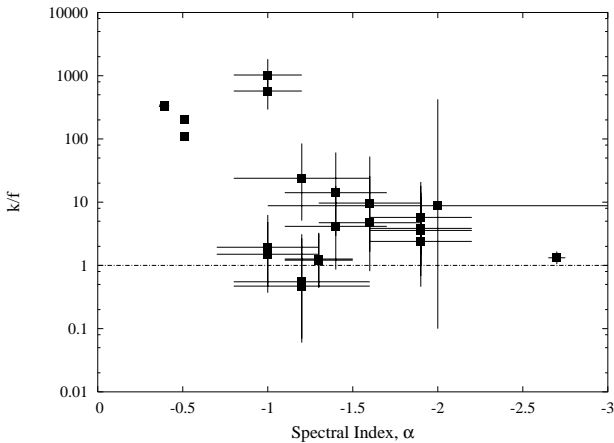


Figure 7. The distribution of k/f versus α . The errors in k/f come from the uncertainty in α .

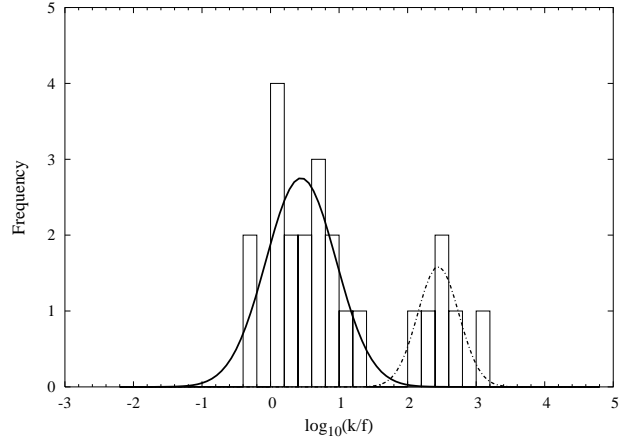


Figure 8. The distribution of the numbers of bubbles with given $\log_{10}(k/f_{\text{sound}})$ values along with the best fitting Gaussian distributions from least-squares analysis.

a $\log_{10}(k/f_{\text{sound}})$ values in a given range were binned (Fig. 8). The distribution appears to be bimodal, with a sample size for the distribution of 23. When the lower populations' values are at the maximum allowed by their uncertainty and the higher populations' values at their minimum, the two populations overlap. Therefore there may be a continuous distribution of k/f_{sound} which we have not seen as our sample size is small. However, with the uncertainties that we have quoted on k/f then no conclusions can be definite. The distribution of k/f values from all timescales was tested using the *EMMIX*¹ program, a more recent version of the KMM algorithm described in Ashman et al. (1994), which uses expectation maximisation to perform a maximum likelihood calculation. The values from the sound speed argument are most likely to be described by a bimodal Gaussian distribution, however the buoyancy values are best fitted by a trimodal distribution, and the refilling values are all but equally likely to be fitted by two, three and four populations. However, all are unlikely to be described by a single Gaussian in log space. The binned k/f values for all of the physical timescale calculations are shown in Fig. 9 for comparison.

The data from the sound speed were then fitted using least squares by two Gaussians, which are shown in the Fig. 8, with means of $\log_{10}(k/f_{\text{sound}}) = 0.44 \pm 0.09$ and 2.45 ± 0.06 (~ 2.3 and ~ 280). The clustering analysis produced the following means $\log_{10}(k/f_{\text{sound}}) = 0.44$ and $= 2.51$ (~ 2.8 and ~ 320), which are within the range from the uncertainties given by least squares fitting.

In order to allow the discussion of a bimodal population of k/f it was investigated whether it was possible to obtain lower limits on k/f for the upper population. If a lower limit could be obtained and is larger than the upper limits of the lower population then the bimodality of the distribution of k/f can be discussed with more reliability.

A lower limit was obtained using the ghost bubbles in Perseus, the only cluster where this is possible to some degree of accuracy. A calculation similar to that for the upper limits was used and the results are shown in Table 4. As there is no GHz radio emission from the ghost bubbles, the electrons have all aged. Therefore the age of the bubble must be *longer* than synchrotron cooling time of the GHz electrons. Radio emission at 330 MHz was analysed

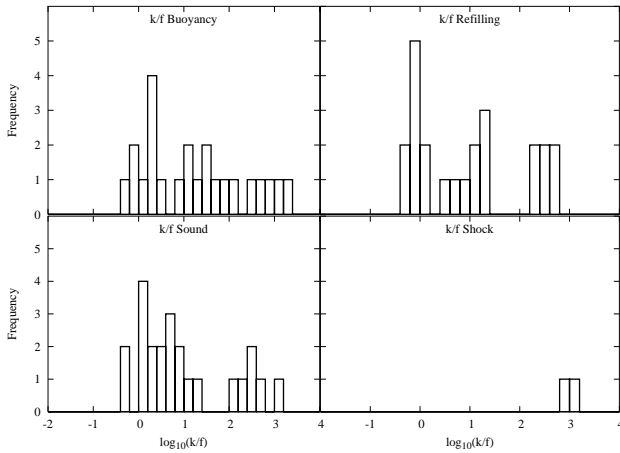
¹ <http://www.maths.uq.edu.au/~gjm/emmix/emmix.html>

Table 4. : LOWER LIMITS ON k/f FROM GHOST BUBBLES IN PERSEUS

Lobe ¹	k/f				Timescales, 10^7 yr			
	k/f_{eq}	k/f_{sound}	k/f_{buoyancy}	k/f_{refill}	$t_{\text{CMB}}^{(2)}$	t_{sound}	t_{buoy}	t_{refill}
West	4271	2267	252	350	13.9	0.795	7.53	5.42
South	4460	1337	304	346	13.9	1.59	7.15	6.27
North	3996	573	1031	278	13.9	2.18	1.19	4.50
South	7262	1025	1682	453	13.9	2.15	1.30	4.90

NOTES:

- (1) The lower limits on k/f for Ghost Bubbles in the Perseus Cluster (West and South). The inner bubbles' values for the upper limits on k/f are shown for comparison (North and South).
- (2) The timescale for the bubble calculated from the magnetic field which produces the same energy density as that of the CMB at the redshift of the cluster for electrons radiating at 1 GHz


Figure 9. The distribution of the numbers of bubbles with given $\log_{10}(k/f)$ values for the sound speed, buoyancy, refilling and shock timescale calculations.

to obtain the energy in electrons radiating between $\nu_1 = 10$ MHz and $\nu_2 = 10$ GHz (see Equation 1) using a steep spectral index of $\alpha = -2.0 \pm 0.5$.

The calculation assumes that the electron distribution is still described by a single spectral index over the above range of frequencies. These lower limits on k/f are above most of the upper limits on k/f obtained for the lower population in Figure 8 (ignoring errors on the limits). There are again discrepancies in the timescales, mainly due to the fact that the sound speed timescale measures the expansion time of the bubble while the buoyancy timescale measures the travel time to the bubbles' current location. In some cases the lower limit obtained is larger than the upper limits for the inner lobes. However, if the ranges in the limits are included then there is overlap between the limits. Also, it is reasonable to use the limit on k/f calculated from the buoyancy timescale rather than the sound speed timescale as the lower limit, as these bubbles have detached from the centre and so are rising buoyantly through the ICM. Using this timescale, the lower limits on k/f are lower than the upper limits from the younger bubbles.

From the observation that there is smooth spectral ageing across the inner lobes (Fabian et al. 2002) and no GHz emission from the outer ghost bubbles we are able, in the special case of the Perseus cluster, to obtain lower as well as upper limits on the value for k/f . It is constrained to be between ~ 100 and ~ 1000 with the assumption that there is no large change in resulting from the

bubbles' detaching from the central engine or its age. The upper limits on k/f for most of the other clusters in the sample are not compatible with this range, which implies that there is at least a large spread in the values for k/f , if not a bimodal distribution. Although the sample size is small (23) we now go on to discuss the implications of a bimodal distribution.

6 INTERPRETATION

To obtain a high value of k/f then either k is intrinsically high or $f \ll 1$. If $f \sim 1$, then k is high and the particles corresponding to the observed synchrotron radio emission do not account for all the particles required for there to be pressure equilibrium. Hence, for M84, Perseus and PKS 1404-267, all of which have high values for k/f , the number of particles emitting synchrotron radiation are not sufficient for the bubble to be in pressure equilibrium. These bubbles, of course, may not be in pressure equilibrium, however the lack of particles would imply that the bubbles are collapsing, which assuming that they are still “powered,” is unlikely. The extra particles required could come from various sources – particles radiating at energies less than 10 MHz, any non-relativistic (thermal) component which has been swept up into the bubbles during their creation and also turbulence. If the jet creating the bubbles were electron-proton, then the protons would be undetectable from the radio emission alone, however they would exert a pressure on the surrounding ICM, and so could account for the extra pressure in the bubble. This implies that there are two types of jets producing radio bubbles — heavy, electron-proton jets giving a high value for k/f , and light, electron-positron jets giving a low value for k/f . Both types of jets have been discussed in the past — Celotti & Fabian (1993) present arguments based on the physical properties of parsec scale radio sources that radio jets are electron-proton; whereas Reynolds et al. (1996) argue that, at least for M87, the jets are electron-positron.

Another effect may be due to the spectral ageing of the electrons in the radio plasma. Once the bubble plasma is no longer “powered” then the electrons will radiate away their energy, with the highest energy ones losing their energy quickest. Assuming an initial power law spectrum, the spectrum will steepen at the high frequency end. If the spectral index that has been used in the calculations comes from the part of the spectrum that has steepened, as it is extrapolated back down to 10 MHz, the value for the flux emitted at lower energies will be an overestimate. Therefore the number of lower-energy particles will also be overestimated, and so pressure equilibrium would seem to be achieved with the “observed” particles, so giving a low k value, even though these particles do not

exist and k is high. This would imply that the low values for k/f obtained for some clusters are because a spectral index that is too steep has been used in the calculation. MKW3s and A133 could be such sources. Their bubbles appear to have detached, they have very steep spectral indices and their k/f values are consistent with one. However the radio emission from other bubbles do not have unusually steep spectra and hence it is unlikely that this situation occurs in the majority of the bubbles.

If f is allowed to vary, then it would be possible to obtain a high k/f with a low k , so the particle energy factors are the same for all clusters, and all that varies is the volume filling factor. Using the means of the two Gaussian distributions from Section 5, a volume filling fraction of ~ 0.01 for the clusters with a higher k/f value would mean that their k values were around 2 – 3, similar to the other sources. However this begs the question – why do there seem to be two types of bubbles – ones with $f \sim 1$ and ones with $f \sim 0.01$? A bimodal distribution seems unlikely in this case, and therefore if the variation in k/f is due to variation on f then there is probably a continuum, possibly shown by k/f_{buoy} , and the clusters that we have chosen appear to give a bimodal distribution of k/f_{sound} . If the distribution of the radio-emitting plasma were filamentary, then f may have a value ~ 0.01 , and a number of radio lobes do show filamentary structure, e.g. Fornax A (Fomalont et al. 1989), M87 (Owen et al. 2000) and Cygnus A (Perley et al. 1984).

In Section 2.1 we have calculated the effect of a simple non-uniform magnetic field, which approximately doubled the value of k/f over that obtained from a uniform field. Hence if the magnetic field were highly non-uniform then the k/f value may increase a substantial amount. As the radio emission is filamentary in some of the lobes which have been analysed, the magnetic field may be as well.

A combination of the two effects may also fit the data. Fabian et al. (2003b) showed that the ghost bubbles in Perseus drag up thermal gas ($H\alpha$) as they rise through the ICM. If this gas is also entrained and mixed with the relativistic plasma during the creation of the bubbles, then the volume filling factor of the radio plasma would be less than one, and, there are extra particles present, meaning that k would be greater than one. This would also imply that there is some evolution of k/f with time, however plotting the k/f value against the corresponding timescale shows no clear correlation. However Schmidt et al. (2002) state that the lobes are essentially devoid of thermal gas, though if it were hotter than ~ 11 keV it would not have been detected.

The rôle of f could also be an explanation, i.e. whether f represents the fraction of the volume of the bubble which is occupied by radio plasma, and the remainder is thermal gas, or whether f is the fraction of the volume filled with detectable radio emitting plasma, and the remainder in this case is filled with relativistic plasma where the electrons (and positrons) have aged, but the magnetic field (and protons) have not lost any of their energy. For the sources with a low k/f and where the radio emission does not fully occupy the X-ray bubble, e.g. A2052, rather than using the flux from the total observed radio emission, the flux from the lower surface brightness region were used. Interpolating this over the whole volume would mean that fewer particles would be inferred from the radio emission, and so the value for k/f would increase.

6.1 Re-acceleration

For there to be re-acceleration in the bubble the magnetic field has to be sufficiently strong. In this case the synchrotron cooling time of the electrons could be very short and we would not expect to

detect GHz emission from the bubble. Nevertheless, if there is re-acceleration then the electrons may still be radiating, from this we would infer a long cooling time. Combining Equations 2 and 3 in the regime where the B^2 term is small enough to be ignored, then $k/f \propto t_{\text{synch}}^{-1}$, and so an inferred cooling time that is long would lead to a limit on k/f that is lower than appropriate.

This could explain the shape and spread of the distribution of the limits on k/f . If the bubbles which have a limit on k/f which is small have ongoing re-acceleration of electrons, then even though the cooling time is short, they have detectable radio emission. Hence we have assumed that the cooling time is long, of order the age of the bubble, and so the calculated limit on k/f is smaller than if the actual cooling time had been used. In this case the bubbles which have a limit on k/f which is large have comparatively little re-acceleration, and the limits on k/f obtained are close to those which have been used in the literature.

The limits on k/f cannot be raised indefinitely – there is a maximum value for the limit (Section 2). However if all the bubbles whose limit on k/f is in the lower population of the bimodal distribution arising from the lack of strong shocks in the rims have their limit on k/f raised to the maximum possible, whereas the others remain where they are; then a multimodal distribution is no more likely than a single Gaussian. The increase in the magnetic field required to raise the limits on k/f to their maximum range from 1.5 (A2199, I-E) to 15 (Cygnus A, E) times that of the one inferred from the synchrotron cooling time with no re-acceleration. These fields lead to cooling times for 1 GHz electrons that are 0.54 to 0.017 times those inferred from the age of the bubble. Hence many cycles of re-acceleration are required such that the electrons are detected, however ~ 60 cycles seems unlikely.

There are two possibilities for how re-acceleration occurs – either there is a population of electrons whose number is almost fixed, and they are re-accelerated repeatedly many times over the age of the bubble so that they are still radiating today. As the radio luminosity $L_{\text{radio}} \propto N_0 B^{1-\alpha} \nu^\alpha dV$, then for a given luminosity, if the magnetic field is stronger, then there are fewer electrons present. If the electrons are re-accelerated, then it is likely that other particles present (e.g. protons & ions) will also be re-accelerated. This would have a minimal effect on k/f as, although there are fewer particles present, they have a higher energy from the re-acceleration. These two effects cancel each other out to some extent and so k is about the same. There are no new extra particles present in the bubble in this case, and so f of the synchrotron emitting plasma is also about the same, hence there is little change in k/f and so this is unlikely as an explanation.

In the other case the electrons are re-accelerated once, in a hotspot say, and then flow throughout the bubble where they age rapidly, but are continuously replaced and so there is still radio emission present today. Cygnus A has a radio structure which seems to match the latter explanation – i.e. the strongest radio emission is at the hotspot, and then the image appears to show that the plasma flows away and becomes less radio bright. In this explanation there would be a population of aged electrons which reduces the volume filling fraction of the emitting relativistic plasma and increases k as the aged electrons also exert a pressure. In this case we only detect $\sim t_{\text{sync}}/t_{\text{bubble}}$ of the particles present. The problem with this model is that for the electrons to flow throughout the bubble before they age they have to travel at $\sim 0.3c$ (for a cooling time of $\sim 10^5$ yr and a bubble radius of 5 kpc).

7 CONCLUSIONS

From a sample of low redshift clusters with clear radio bubbles which are coincident with decrements in the X-ray emission, we have determined limits on k/f , where k is the ratio of the total relativistic particle energy to that in electrons radiating between 10 MHz to 10 GHz and f is the volume filling factor of the relativistic plasma. We find that no bubble has simple equipartition between the pressures from the relativistic particles and the magnetic field. k/f was found to have no strong dependence on any physical parameter of the host cluster, however there seemed to be two populations. One set of clusters had a k/f value around 2, the remainder had a value of around 300. This apparent bimodality of the distribution of k/f could be explained in various ways. The jets creating the bubbles are of two types — electron-positron, which would have a low value for k (for $f \sim 1$), and electron-proton, where the protons are the extra particles required to maintain pressure equilibrium, but as they are unseen in the radio emission k is high. Spectral ageing of the radio plasma steepens the spectrum, so giving the impression that there are more particles present. A bimodality in the volume filling fraction which could be caused by either a non-uniform magnetic field, or a filamentary structure in the lobes. If thermal plasma is entrained during the formation of the bubbles this would reduce the volume filling factor and provide extra particles, resulting in the calculated values. Variations in the amounts of re-acceleration may also produce the observed distribution.

ACKNOWLEDGMENTS

We thank Greg Taylor for valuable help with obtaining some of the radio images, Annalisa Celotti for helpful discussions, Guy Pooley and Rosie Bolton for guidance with AIPS, and the referee, Eugene Churazov, for many helpful comments and suggestions. ACF and RJHD acknowledge support from The Royal Society and PPARC respectively.

REFERENCES

- Alexander P., Brown M. T., Scott P. F., 1984, MNRAS, 209, 851
 Andernach H., Han Tie, Sievers A., Reuter H.-P., Junkes N., Wielebinski R., 1988, A&AS, 73, 265
 Ashman K. A., Bird C. M., Zepf S. E., 1994, AJ, 108, 2348
 Birzan L., Rafferty D. A., McNamara B. R., Wise M. W., Nulsen P. E. J., 2004, ApJ, 607, 800
 Bettoni D., Falomo R., Fasano G., Govoni F., 2003, A&A, 399, 869
 Blanton E. L., Sarazin C. L., McNamara B. R., 2003, ApJ, 585, 227
 Blanton E. L., Sarazin C. L., McNamara B. R., Wise M. W., 2001, ApJ, 558, L15
 Böhringer H., Voges W., Fabian A. C., Edge A. C., Neumann D. M., 1993, MNRAS, 264, L25
 Brown D. L., Burns J. O., 1991, AJ, 102, 1917
 Burbidge G. R., 1959, ApJ, 129, 849
 Burns J. O., 1990, AJ, 99, 14
 Burns J. O., Schwendeman E., White R. A., 1983, ApJ, 271, 575
 Cao X., Rawlings S., 2004, MNRAS, 349, 1419
 Carilli C. L., Perley R. A., Dreher J. W., Leahy J. P., 1991, ApJ, 383, 554
 Celotti A., Fabian A. C., 1993, MNRAS, 264, 228
 Choi Y., Reynolds C. S., Heinz S., Rosenberg J. L., Perlman E. S., Yang J., 2004, ApJ, 606, 185
 Churazov E., Brüggén M., Kaiser C. R., Böhringer H., Forman W., 2001, ApJ, 554, 261
 Churazov E., Forman W., Jones C., Böhringer H., 2000, A&A, 356, 788
 Drinkwater M. J. et al., 1997, MNRAS, 284, 85
 Fabian A. C., Celotti A., Blundell K. M., Kassim N. E., Perley R. A., 2002, MNRAS, 331, 369
 Fabian A. C., Sanders J. S., Allen S. W., Crawford C. S., Iwasawa K., Johnstone R. M., Schmidt R. W., Taylor G. B., 2003a, MNRAS, 344, L43
 Fabian A. C., Sanders J. S., Crawford C. S., Conselice C. J., Gallagher J. S., Wyse R. F. G., 2003b, MNRAS, 344, L48
 Fabian A. C. et al., 2000, MNRAS, 318, L65
 Finoguenov A., Jones C., 2002, ApJ, 574, 754
 Fomalont E. B., Ebner K. A., van Breugel W. J. M., Ekers R. D., 1989, ApJ, 346, L17
 Forman W. et al., 2003, astro-ph/0312576
 Fujita Y., Sarazin C. L., Kempner J. C., Rudnick L., Slee O. B., Roy A. L., Andernach H., Ehle M., 2002, ApJ, 575, 764
 Johnstone R. M., Allen S. W., Fabian A. C., Sanders J. S., 2002, MNRAS, 336, 299
 Johnstone R. M., Fabian A. C., Taylor G. B., 1998, MNRAS, 298, 854
 Komissarov S. S., Gubanov A. G., 1994, A&A, 285, 27
 Mazzotta P., Kaastra J. S., Paerels F. B., Ferrigno C., Colafrancesco S., Mewe R., Forman W. R., 2002, ApJ, 567, L37
 McNamara B. R., O'Connell R. W., Bregman J. N., 1990, ApJ, 360, 20
 McNamara B. R. et al., 2000, ApJ, 534, L135
 Owen F. N., Eilek J. A., Kassim N. E., 2000, ApJ, 543, 611
 Owen F. N., Ledlow M. J., 1997, ApJS, 108, 41
 Pedlar A., Ghataure H. S., Davies R. D., Harrison B. A., Perley R., Crane P. C., Unger S. W., 1990, MNRAS, 246, 477
 Perley R. A., Dreher J. W., Cowan J. J., 1984, ApJ, 285, L35
 Reiprich T. H., Böhringer H., 2002, ApJ, 567, 716
 Reynolds C. S., Fabian A. C., Celotti A., Rees M. J., 1996, MNRAS, 283, 873
 Rizza E., Loken C., Bliton M., Roettiger K., Burns J. O., Owen F. N., 2000, AJ, 119, 21
 Sanders J. S., Fabian A. C., 2002, MNRAS, 331, 273
 Schmidt R. W., Fabian A. C., Sanders J. S., 2002, MNRAS, 337, 71
 Slee O. B., Reynolds J. E., 1984, Proceedings of the Astronomical Society of Australia, 5, 516
 Slee O. B., Roy A. L., Murgia M., Andernach H., Ehle M., 2001, AJ, 122, 1172
 Smith D. A., Wilson A. S., Arnaud K. A., Terashima Y., Young A. J., 2002, ApJ, 565, 195
 Stefanachi F., Venturi T., Dallacasa D., 2002, in Proceedings of the 6th EVN Symposium, p. 147
 Taylor G. B., Barton E. J., Ge J., 1994, AJ, 107, 1942
 Taylor G. B., Fabian A. C., Allen S. W., 2002, MNRAS, 334, 769
 Taylor G. B., Perley R. A., Inoue M., Kato T., Tabara H., Aizu K., 1990, ApJ, 360, 41
 Teräsranta H., Urpo S., Wiren S., Valtonen M., 2001, A&A, 368, 431
 Voigt L. M., Fabian A. C., 2004, in prep
 Zhao J., Sumi D. M., Burns J. O., Duric N., 1993, ApJ, 416, 51

Table 5. TIMESCALES AND POWERS

Cluster	Lobe ⁽¹⁾	$t_{\text{CMB}}^{(2)}$ 10^6 yr	t_{sound} 10^7 yr	t_{shock} 10^7 yr	t_{buoy} 10^7 yr	t_{refill} 10^7 yr	t_{min} 10^7 yr	t_{max} 10^7 yr	$\mathcal{P}_{\text{sound}}^{(3)}$ $10^{43} \text{ ergs}^{-1}$	$\mathcal{P}_{\text{shock}}$ $10^{43} \text{ ergs}^{-1}$	$\mathcal{P}_{\text{buoy}}$ $10^{43} \text{ ergs}^{-1}$	$\mathcal{P}_{\text{refill}}$ $10^{43} \text{ ergs}^{-1}$
A133	Rel, R	12.38	13.9	-	1.99	6.93	1.26	1.22	4.74	-	33.1	9.52
A2052	N, X	13.21	4.11	-	0.39	1.49	0.68	0.26	1.80	-	18.8	4.98
	S, X	13.21	6.16	-	0.65	2.44	1.03	0.43	4.06	-	38.6	10.2
A2199	E, R	13.36	4.14	-	1.98	5.30	0.50	0.93	3.20	-	6.70	2.50
	W, R	13.36	5.04	-	1.91	5.82	0.58	1.03	4.47	-	11.8	3.86
	I-E, R	13.36	0.30	-	1.54	1.37	0.05	0.24	0.05	-	0.01	0.01
	I-W, R	13.36	0.45	-	1.26	1.68	0.075	0.30	0.12	-	0.04	0.03
A4059	N, R	12.65	1.66	-	0.25	0.71	0.15	0.13	0.12	-	0.80	0.29
	S, R	12.65	1.19	-	0.18	0.74	0.23	0.13	0.58	-	3.77	0.93
Centaurus	E, R	14.19	0.70	-	0.31	1.02	0.091	0.18	0.02	-	0.05	0.01
	E, R	14.19	0.81	-	0.46	1.20	0.073	0.21	0.01	-	0.03	0.01
Cygnus A	E, R	12.43	6.53	-	5.09	11.7	0.85	2.06	56.3	-	72.2	31.5
	W, R	12.43	6.23	-	4.41	10.1	0.77	1.79	77.5	-	109	47.7
Hydra A	N, R	12.57	5.04	-	1.25	3.44	0.35	0.61	1.98	-	8.00	2.90
	S, R	12.57	4.16	-	2.13	3.87	0.28	0.68	1.16	-	2.26	1.24
M84	N, R	14.48	1.12	-	0.40	0.74	0.23	0.13	0.05	-	0.21	0.08
	S, R	14.48	2.14	-	0.56	1.05	0.23	0.19	0.03	-	0.16	0.06
M87	Bud, R	14.45	0.46	-	0.55	0.89	0.077	0.16	0.20	-	0.16	0.10
MKW3s	S, R	12.83	3.11	-	5.52	5.60	0.72	0.99	3.22	-	1.81	1.79
Perseus	N, X	13.87	2.18	3.20	1.19	4.50	0.36	0.80	5.70	3.87	10.4	2.75
	S, X	13.87	2.15	2.90	1.30	4.90	0.36	0.87	7.84	5.81	13.0	3.44
PKS1404	E, X	13.72	1.02	-	0.40	0.74	0.12	0.13	0.03	-	0.07	0.04
	W, X	13.72	0.63	-	0.26	0.53	0.14	0.094	0.06	-	0.14	0.07

NOTES:

(1) The codes for the Lobes are N—Northern, S—Southern, E—Eastern, W—Western, X—sizes from X-ray image, R—sizes from Radio image, I-E/W—Inner lobes in A2199, Bud—as described in Forman et al. (2003), Rel—Relic source as described in Fujita et al. (2002).

(2) The timescale for the bubble calculated from the magnetic field which produces the same energy density as that of the CMB at the redshift of the cluster for electrons radiating at 1 GHz.

(3) The power is the PV/t work only, with $\frac{\gamma}{\gamma-1}$ not accounted for. Therefore, for a fully relativistic plasma the values for the powers need to be multiplied by four, and for a non-relativistic plasma, by 5/2.

APPENDIX

The bubble timescales and derived powers are presented in Table 5.